ARRAY GEOMETRY OPTIMIZATION FOR REGION-OF-INTEREST NEAR-FIELD BEAMFORMING

Ron Moisseev, Gal Itzhak, and Israel Cohen

Andrew and Erna Viterbi Faculty of Electrical and Computer Engineering
Technion – Israel Institute of Technology, Haifa 3200003, Israel

ABSTRACT

Microphone array geometry plays a crucial role in array signal processing and beamforming. This paper presents an array geometry optimization approach for near-field beamforming. Considering a continuous region of interest, we aim to maximize the worst-case broadband directivity of the array while ensuring sufficiently high white noise gain. We use a near-field wave propagation analysis to formulate a convex optimization problem and find the optimal linear array topology. We evaluate the performance of the proposed approach for different desired signal directions and distances and compare our results to traditional beamformers. The optimized non-uniform geometry achieves better white noise gain and higher array directivity than standard uniform linear arrays. Furthermore, the proposed method can be used for near- and far-field sources.

***Index Terms*—** Array signal processing, region-of-interest near-field beamforming, array geometry optimization.

1. INTRODUCTION

Microphone arrays use optimal beamforming to enhance speech and reduce noise [1–3], detect and localize sources [4–6], and recognize speech [7, 8]. Traditionally, beamforming enhances signals of interest while attenuating undesirable background noise by exploiting spatial information captured by the array [9–12]. Each microphone signal is filtered according to an assumed wave propagation model considering the array's geometry.

Conventional far-field signal models assume that the source is far enough from the microphone array to approximate the acoustic wave as a plane wave. As a result, the signals measured by each microphone differ only by a phase shift [2]. However, this far-field assumption is not valid when the array's aperture is large or when the array is close to the source, relative to the wavelength of the signal [13]. A near-field model expresses the signal's phase and amplitude in these scenarios. Such a model is standard in various fields, including ultrasound imaging [14], opto-acoustics [15], and radar imaging [16].

Improving beamforming performance is done by fine-tuning the filter coefficients and optimizing the array geometry. While the coefficients can be adjusted in real-time, the array geometry is typically fixed after manufacturing. Thus, careful considerations need to be made when choosing microphone placements. Naturally, with near-field beamforming designs, uniformly spaced geometries are employed. These geometries include, for example, uniform linear arrays (ULAs) [17] and uniform rectangular arrays (URAs) [18], which are the simplest to implement, albeit very rarely provide an optimal selection concerning any of the standard performance criteria.

Array geometry optimization methods may be applied to generate customized arrays that are optimal concerning specific criteria. In recent years, array optimization techniques were demonstrated in the far-field [19] and near-field [20, 21] regimes. They often use time-consuming Monte Carlo simulations [22], neural network optimization methods [23], or genetic algorithms [24, 25] to randomly search for an optimal geometry. Convex optimization [26–28] provides a way to guarantee a globally optimal solution much more efficiently [29]. These optimized arrays were shown to potentially improve the white noise gain (WNG) or the array directivity compared to the traditional non-optimized designs.

This paper presents a method for designing a near-field beamformer considering a continuous two-dimensional region of interest (ROI) in space. First, we introduce an optimization scheme to determine the optimal microphone placements for a given ROI. Then, we calculate the beamformer coefficients for a known source position. At some level, this work may be regarded as a generalization of a previous study [26], which considers far-field signals. We aim to maximize the directivity factor (DF) while maintaining an adequate WNG and considering the array's physical limitations. The proposed approach is shown to outperform standard designs in terms of directivity and WNG, and may also be used for far-field sources.

The rest of the paper is organized as follows. We formulate the signal model in Section 2. In Section 3, we present the optimization variables and the target function, and describe the array optimization process. Finally, in Section 4, we demonstrate the advantages of the proposed approach compared to a dense configuration and examine the optimized array for signals originating in the far-field.

2. SIGNAL MODEL

Consider a signal of interest $X(\omega)$ originating from $\mathbf{r}_s \in \mathbb{R}^3$ and propagating in free space at the speed of sound c. The signal impinges on a linear microphone array of M omnidirectional microphones, with the i-th microphone positioned at $\mathbf{x}_i \in \mathbb{R}^3$. The free-field Green function, describing the propagation of the signal from the source position to the microphone position, is given by [30]:

$$g_{s,i}(\omega) = g(\mathbf{r}_s, \mathbf{x}_i, \omega) = \frac{e^{-j\omega\|\mathbf{r}_s - \mathbf{x}_i\|/c}}{4\pi\|\mathbf{r}_s - \mathbf{x}_i\|} \tag{1}$$

where $\|\cdot\|$ is the Euclidean norm, $\omega = 2\pi f$ is the angular frequency, f is the temporal frequency and j is the imaginary unit. This function should be used when the microphone is in the near-field of the

e-mail: {m.ron@campus.technion.ac.il, galitz@technion.ac.il, icohen@ee.technion.ac.il}.

This research was supported by the Israel Science Foundation (grant no. 1449/23) and the Pazy Research Foundation.

source, which are all the points whose distance $\hat{r}$ from the source satisfies [13]:

$$\hat{r} < A^2/\lambda \tag{2}$$

where A is the aperture of the array and $\lambda = c/f$ is the signal's wavelength.

The measured signal in the frequency domain is expressed by:

$$\begin{aligned} \mathbf{y}(\omega) &= \begin{bmatrix} Y_1(\omega) & Y_2(\omega) & \cdots & Y_M(\omega) \end{bmatrix}^T \\ &= \mathbf{d}(\mathbf{x}, \mathbf{x}_{\text{ref}}, \mathbf{r}_s, \omega) X(\omega) + \mathbf{v}(\omega) \end{aligned} \tag{3}$$

where the superscript ^{T} is the transpose operator, $Y_i(\omega)$ is the measured signal at the i-th microphone,

$$\mathbf{d}(\mathbf{x}, \mathbf{x}_{\text{ref}}, \mathbf{r}_s, \omega) = \begin{bmatrix} \frac{g_{s,1}(\omega)}{g_{s,\text{ref}}(\omega)} & \frac{g_{s,2}(\omega)}{g_{s,\text{ref}}(\omega)} & \cdots & \frac{g_{s,M}(\omega)}{g_{s,\text{ref}}(\omega)} \end{bmatrix}^T \tag{4}$$

is the array steering vector, $\mathbf{x} = \left[\mathbf{x}_1^T, \mathbf{x}_2^T, \cdots, \mathbf{x}_M^T\right]^T$ is the microphone positions vector of length $3M$, $\mathbf{x}_{\text{ref}}$ is the reference microphone position, and $\mathbf{v}(\omega)$ is the additive noise vector.

3. ARRAY GEOMETRY OPTIMIZATION

3.1. Near-Field Beamforming

Given an array of microphones whose locations are specified by the elements of $\mathbf{x}$, we can construct a beamformer of length M denoted by $\mathbf{h}(\mathbf{x}, \mathbf{r}_s, \omega)$. The output of the beamformer for a source signal originating from $\mathbf{r}_s$ is given by:

$$\hat{X}(\omega) = \mathbf{h}^H(\mathbf{x}, \mathbf{r}_s, \omega)\, \mathbf{y}(\omega) \tag{5}$$

where the superscript ^{H} is the conjugate-transpose operator.

We employ two common performance measures to evaluate the beamformer's sensitivity. The first performance measure, describing the robustness of the array to spatially white noise, is the (narrowband) WNG:

$$\mathcal{W}[\mathbf{h}(\mathbf{x}, \mathbf{r}_s, \omega)] = \frac{\left|\mathbf{d}^H(\mathbf{x}, \mathbf{x}_{\text{ref}}, \mathbf{r}_s, \omega)\, \mathbf{h}(\mathbf{x}, \mathbf{r}_s, \omega)\right|^2}{\mathbf{h}^H(\mathbf{x}, \mathbf{r}_s, \omega)\, \mathbf{h}(\mathbf{x}, \mathbf{r}_s, \omega)}. \tag{6}$$

The second performance measure is the (narrowband) DF, which quantifies the robustness of the array to a spatially-isotropic diffuse noise field originating in the far-field. It is given by:

$$\mathcal{D}[\mathbf{h}(\mathbf{x}, \mathbf{r}_s, \omega)] = \frac{\left|\mathbf{d}^H(\mathbf{x}, \mathbf{x}_{\text{ref}}, \mathbf{r}_s, \omega)\, \mathbf{h}(\mathbf{x}, \mathbf{r}_s, \omega)\right|^2}{\mathbf{h}^H(\mathbf{x}, \mathbf{r}_s, \omega)\, \mathbf{\Gamma}(\mathbf{x}, \omega)\, \mathbf{h}(\mathbf{x}, \mathbf{r}_s, \omega)}, \tag{7}$$

where $\mathbf{\Gamma}(\mathbf{x}, \omega)$ is given by:

$$\Gamma_{i,j}(\mathbf{x}, \omega) = \frac{\sin\left(\omega\left(\|\mathbf{x}_i - \mathbf{x}_j\|/c\right)\right)}{\omega\left(\|\mathbf{x}_i - \mathbf{x}_j\|/c\right)}. \tag{8}$$

Finally, the narrowband DF may be extended to the broadband directivity index by defining the following:

$$\mathcal{DI}_{[\omega_l, \omega_h]}[\mathbf{h}(\mathbf{x}, \mathbf{r}_s, \omega)] = \frac{\int_{\omega_l}^{\omega_h} \left|\mathbf{d}^H(\mathbf{x}, \mathbf{x}_{\text{ref}}, \mathbf{r}_s, \omega)\, \mathbf{h}(\mathbf{x}, \mathbf{r}_s, \omega)\right|^2}{\int_{\omega_l}^{\omega_h} \mathbf{h}^H(\mathbf{x}, \mathbf{r}_s, \omega)\, \mathbf{\Gamma}(\mathbf{x}, \omega)\, \mathbf{h}(\mathbf{x}, \mathbf{r}_s, \omega)} \tag{9}$$

where ω_h and ω_l are the maximal and minimal frequencies in the source spectrum, respectively.

3.2. Optimization Variables

Our objective is to find the optimal microphone layout $\mathbf{x}^*$ that maximizes the worst-case directivity index (9) in a general ROI. The optimization is done under the constraints of distortionless response, sufficient WNG (6), and a minimal distance d_c between adjacent microphones. Inspired by [26], we construct a convex optimization problem with discrete variables.

First, we define an ROI in a two-dimensional Cartesian grid using r and θ, and assume that it is bounded by $r \in [r_l, r_h]$ and $\theta \in [\theta_l, \theta_h]$. The set of all possible source locations, $\mathbf{r}_{s,p}$, are located on a discrete grid defined as:

$$\begin{aligned} &\mathbf{r}_{s,p} = (r_s \cos\theta_p, r_s \sin\theta_p), \\ &\theta_p = \theta_l + \frac{\theta_h - \theta_l}{P-1}(p-1),\ r_s = r_l + \frac{r_h - r_l}{S-1}(s-1), \\ &p \in [1, P], \quad s \in [1, S], \end{aligned} \tag{10}$$

where P and S are the total number of sampled grid points of θ and r, respectively. Furthermore, the sampled frequency grid of the band-limited signal is defined as:

$$\omega_q = \omega_l + \frac{\omega_h - \omega_l}{Q-1}(q-1), \quad q \in [1, Q], \tag{11}$$

where Q is the number of frequency grid points.

Next, we assume that the array is situated on the x-axis, e.g., the i-th microphone is located at $\mathbf{x}_i = (x_i, 0)$, and the array's maximum aperture is A. We limit the number of possible microphone locations by sampling the x axis at N, equally spaced, possible locations:

$$\Delta x = \frac{A}{N-1},\ x_i = -\Delta x\,(i-1) \quad i \in [1, N]. \tag{12}$$

Using the vectors defined above and a reference position x_{ref} chosen from (12), we calculate the steering vector $\mathbf{d}(x_{\text{ref}}, r_s, \theta_p, \omega_q)$ for each possible source location $\mathbf{r}_{s,p}$ using (4).

The two optimization variables are the binary selection vector and the filter coefficients vector. The selection vector is defined as:

$$\mathbf{z} = \begin{bmatrix} Z_1 & Z_2 & \cdots & Z_N \end{bmatrix}^T, \tag{13}$$

where Z_i is one if a microphone is present at x_i and zero otherwise.

The filter coefficients vector, representing a beamformer directed towards (r, θ) utilizing all N possible microphone placements, is defined for each sampled grid point (s, p, q) as:

$$\mathbf{h}(r_s, \theta_p, \omega_q) = \begin{bmatrix} H_1(r_s, \theta_p, \omega_q) & H_2(r_s, \theta_p, \omega_q) & \cdots & H_N(r_s, \theta_p, \omega_q) \end{bmatrix}^T. \tag{14}$$

Subsequently, the number of coefficient variables is $N \times P \times Q \times S$.

3.3. Optimization Target Function and Constraints

The optimization objective is to minimize a target function while maintaining desirable constraints. First, we limit the number of placed microphones to M by defining:

$$\mathcal{C}_1[\mathbf{z}] : \mathbf{z}^T \mathbf{i}_N = M, \tag{15}$$

where $\mathbf{i}_N$ is a column vector of length N consisting of ones. Additionally, the minimal space between two adjacent microphones should be d_c:

$$\mathcal{C}_2[\mathbf{z}] : \mathbf{z}^T U = \mathbf{i}_G^T, \tag{16}$$

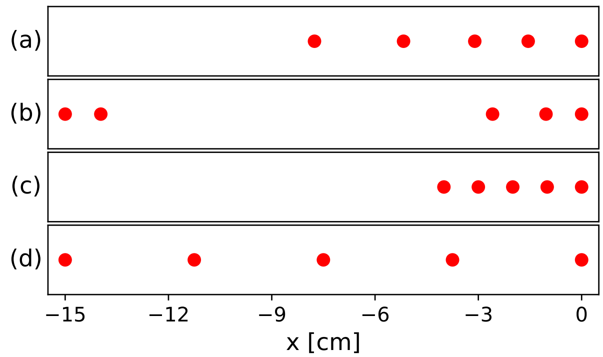

Fig. 1. Different array geometries. (a) Optimal geometry for near-field, (b) Optimal geometry for far-field, (c) Dense geometry, (d) ULA geometry. $M = 5$, $d_c = 1\,\text{cm}$, $A = 15\,\text{cm}$.

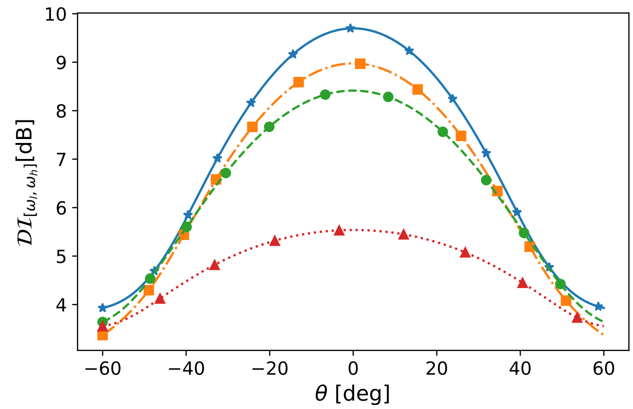

Fig. 2. Directivity index as a function of θ for a source located at $r = 10\,\text{cm}$. The star, square, circle, and triangle markers represent the optimal near-field geometry, dense geometry, optimal far-field geometry, and ULA geometry, respectively.

where $G = N - \lfloor \frac{d_c}{\Delta x} \rfloor$ is the number of restricted areas, $U \in \mathbb{R}^{N\times G}$ is a matrix whose i-th column is:

$$u_i = \begin{bmatrix} \mathbf{0}_{i-1}^T & \mathbf{i}_{N+1-G}^T & \mathbf{0}_{G-i}^T \end{bmatrix}^T, \tag{17}$$

and $\mathbf{0}_{i-1}$ is a column vector consisting zeros of length i.

The subsequent constraints ensure that the beamformer utilizes M microphones and achieves distortionless response while upholding a minimum WNG of δ:

$$\begin{aligned} \mathcal{C}_3\left[\mathbf{h}\right] &: \mathbf{d}^H\left(x_{\text{ref}}, r_s, \theta_p, \omega_q\right)\mathbf{h}\left(r_s, \theta_p, \omega_q\right) = 1, \\ \mathcal{C}_4\left[\mathbf{h}\right] &: \mathbf{h}^H\left(r_s, \theta_p, \omega_q\right)\mathbf{h}\left(r_s, \theta_p, \omega_q\right) \le \frac{1}{\delta}, \\ \mathcal{C}_5\left[\mathbf{z}, \mathbf{h}\right] &: \left|H_i\left(r_s, \theta_p, \omega_q\right)\right|^2 \le \frac{Z_i}{\delta}, \\ &\forall i \in [1, N], \forall p \in [1, P], \forall q \in [1, Q], \forall s \in [1, S]. \end{aligned} \tag{18}$$

Finally, we define the target function for the near-field case. We aim to maximize the worst-case directivity index (9). Constraint $\mathcal{C}_3[\mathbf{h}]$ renders the numerator of (9) constant, simplifying the optimization process to minimizing the following convex function:

$$R[\mathbf{h}] = \max_{\substack{p\in[1,P]\\ s\in[1,S]}} \sum_{q=1}^{Q} \mathbf{h}^H\left(r_s, \theta_p, \omega_q\right)\Gamma\left(\omega_q\right)\mathbf{h}\left(r_s, \theta_p, \omega_q\right), \tag{19}$$

where

$$\Gamma_{i,j}(\omega) = \frac{\sin\left(\omega\left(i-j\right)\Delta x/c\right)}{\omega\left(i-j\right)\Delta x/c}, \quad i,j \in [1, N]. \tag{20}$$

The mixed-integer optimization problem can be solved using various solvers, yielding optimized variables $\mathbf{z}$ and $\mathbf{h}$, whose non-zero elements represent the optimized microphone locations and beamformer coefficients.

3.4. Robust Beamforming

The performance of the beamformer depends on the array geometry and the filter coefficients. While the former is given by the proposed method, the latter needs to be calculated given the source location. In this work, we use the robust superdirective beamformer, which maximizes the DF while maintaining an acceptable minimum value of the WNG. This beamformer corresponds to our optimization objective and constraints and is shown to be an adequate selection in other studies involving the near-field signal model [31,32]. Assuming the source location is known, we construct the beamformer as in [19,26] using the bisection method.

4. EXPERIMENTAL RESULTS

We solve the addressed optimization problem using the Python package CVXPY [33] with the MOSEK solver [34]. The simulations approximate a real-world microphone configuration suitable for use in close proximity to the speaker and are conducted using the following parameters: $M = 5$ microphones at $N = 30$ possible locations over $A = 15\,\text{cm}$, with a minimal distance between adjacent microphones $d_c = 1\,\text{cm}$ and reference microphone $\mathbf{x}_{\text{ref}} = 0$. The variables grid is sampled using $P = 10$, $Q = 10$, $S = 10$ for $1\,\text{KHz} \le f \le 6\,\text{KHz}$, $|\theta| \le 30^\circ$, $5\,\text{cm} \le r \le 15\,\text{cm}$ and the minimum WNG is $\delta = -10\,\text{dB}$. Using (2), the near-field extends up to approximately $40\,\text{cm}$ from the source. This indicates that the near-field assumption is strictly necessary for the described scenario.

Figure 1 illustrates various potential array configurations. The first is the suggested optimal geometry using a near-field model. In this case, the microphones are positioned on the right side, closer to the source. Next is the optimal geometry using the far-field model as in [26]. In contrast to scenario (a), this arrangement also incorporates microphones on the left side. The densely-packed configuration (c) closely resembles (a), with each microphone placed at a distance of d_c from its neighboring microphone. Lastly, (d) represents the ULA that spans the entire potential aperture using equidistantly spaced microphones.

In Figure 2, the broadband directivity index (9) is showcased for a source positioned at $r = 10\,\text{cm}$ and $|\theta| \le 60^\circ$. Among the considered geometries, the optimal near-field arrangement attains the highest directivity index, followed by the dense configuration. Conversely, the optimal far-field geometry and the ULA perform relatively poorly in this context. Interestingly, the optimal near-field geometry demonstrates superior performance across all angles, even those beyond the optimized range.

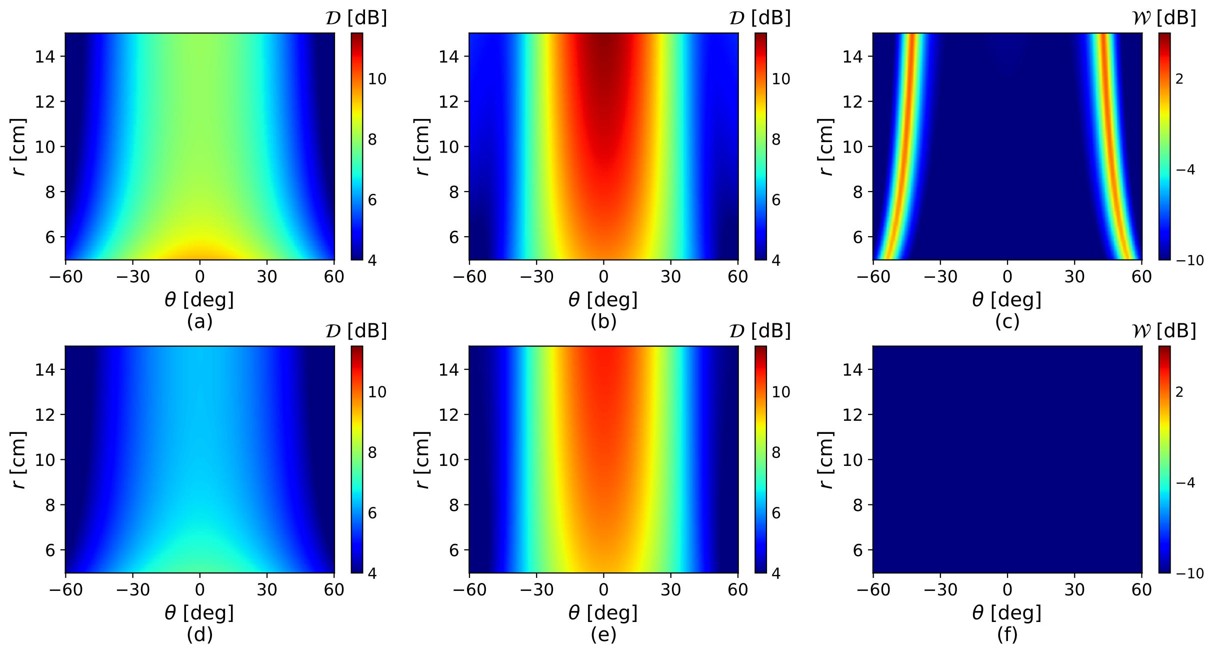

Fig. 3. DF and WNG as a function of r and θ for the optimized and dense geometries. (a) DF for optimized geometry, $f = 1\,\mathrm{KHz}$, (b) DF for optimized geometry, $f = 4.5\,\mathrm{KHz}$, (c) WNG for optimized geometry, $f = 4.5\,\mathrm{KHz}$, (d) DF for dense geometry, $f = 1\,\mathrm{KHz}$, (e) DF for dense geometry, $f = 4.5\,\mathrm{KHz}$, (f) WNG for dense geometry, $f = 4.5\,\mathrm{KHz}$. The WNG for $f = 4.5\,\mathrm{KHz}$ is strictly -10 dB for both beamformers within the entire ROI.

The suggested geometry and the dense configuration exhibit the best directivity index and share similar microphone placements. Further comparison of the DF and WNG between the two configurations is illustrated in Figure 3 for $f = 1\,\mathrm{kHz}$ and $f = 4.5\,\mathrm{kHz}$. At lower frequencies, both configurations achieve the minimum allowable WNG of $-10\,\mathrm{dB}$, but the suggested geometry outperforms the dense configuration in terms of DF for all angles and distances. The highest DF is attained when the source is located near the array. This advantage extends to higher frequencies. While both configurations maintain $-10\,\mathrm{dB}$ WNG within the optimized angle range, the WNG of the proposed geometry increases by up to $2\,\mathrm{dB}$ outside the optimized angle range. Moreover, the DF of the suggested geometry consistently offers superior DF across angles and distances. In comparison to $f = 1\,\mathrm{kHz}$, at $f = 4.5\,\mathrm{kHz}$, the best DF is attained for sources located farther from the array.

Further simulations were conducted to analyze the optimized array for signals originating far from the array. We calculated the optimal geometry with the proposed method for far-field signals by setting $r = 25\,\mathrm{m}$. The resulting array matches the configuration obtained using [26], which is illustrated in Figure 1(b). This implies that our proposed approach may be regarded as a generalization of that approach: when the desired source signal is close to the array, it considers the near-field signal model to describe the nature of the propagating acoustic wave more realistically; however, when the desired source signal is far from the array, the two approaches yield identical solutions.

5. CONCLUSIONS

We have presented a beamforming approach based on linear array geometry optimization for ROI near-field beamforming. The proposed method considers a continuous ROI and maximizes the worst-case broadband directivity index while maintaining a minimal value of the WNG to yield the optimal array geometry. Then, a post-processing stage is employed to derive the optimal robust superdirective beamformer coefficients considering the optimal array geometry. We conducted comprehensive simulations comparing traditional dense and ULA beamformers with our proposed approach. The results indicate that the latter achieves a superior broadband directivity index, and further analysis shows that the proposed approach achieves improved WNG and higher narrowband array directivity compared to the dense array. Moreover, we have simulated a desired source originating in the far field and demonstrated that the proposed approach and the existing far-field geometry optimization approach converge when the desired source signal is far from the array. In future research, we may refine the coefficients post-processing scheme to *a priori* unknown source positions within the ROI, and expand the proposed approach to two- and three-dimensional arrays.

6. REFERENCES

[1] H. L. Van Trees, *Optimum Array Processing: Part IV of Detection, Estimation, and Modulation Theory*, ser. Detection, Estimation, and Modulation Theory. New York: Wiley, 2004.

[2] J. Benesty, I. Cohen, and J. Chen, *Fundamentals of Signal Enhancement and Array Signal Processing*. New York: Wiley-IEEE Press, 2018.

[3] G. Itzhak, J. Benesty, and I. Cohen, "Nonlinear kronecker product filtering for multichannel noise reduction," *Speech Communication*, vol. 114, pp. 49–59, 2019.

[4] J. He, L. Li, and T. Shu, "Localization of near-field sources for

exact source-sensor spatial geometry," *IEEE Signal Processing Letters*, vol. 27, pp. 1040–1044, 2020.

[5] Y.-D. Huang and M. Barkat, "Near-field multiple source localization by passive sensor array," *IEEE Transactions on Antennas and Propagation*, vol. 39, pp. 968–975, 7 1991.

[6] P. Chiariotti, M. Martarelli, and P. Castellini, "Acoustic beamforming for noise source localization–reviews, methodology and applications," *Mechanical Systems and Signal Processing*, vol. 120, pp. 422–448, 2019.

[7] W. Zhang, C. Boeddeker, S. Watanabe, T. Nakatani, M. Delcroix, K. Kinoshita, T. Ochiai, N. Kamo, R. Haeb-Umbach, and Y. Qian, "End-to-end dereverberation, beamforming, and speech recognition with improved numerical stability and advanced frontend," in *2021 IEEE International Conference on Acoustics, Speech and Signal Processing (ICASSP)*, 2021, pp. 6898–6902.

[8] B. J. Cho, J.-M. Lee, and H.-M. Park, "A beamforming algorithm based on maximum likelihood of a complex gaussian distribution with time-varying variances for robust speech recognition," *IEEE Signal Processing Letters*, vol. 26, no. 9, pp. 1398–1402, 2019.

[9] J. Benesty, J. Chen, Y. Huang, and I. Cohen, *Noise Reduction in Speech Processing*, 1st ed. Berlin: Springer-Verlag Berlin Heidelberg, 2009.

[10] G. Itzhak, J. Benesty, and I. Cohen, "On the design of differential Kronecker product beamformers," *IEEE/ACM Transactions on Audio, Speech, and Language Processing*, vol. 29, pp. 1397–1410, 2021.

[11] G. Itzhak, I. Cohen, and J. Benesty, "Robust differential beamforming with rectangular arrays," in *Proc. 29th European Signal Processing Conference, EUSIPCO-2021*, Aug 2021.

[12] G. Itzhak, J. Benesty, and I. Cohen, "Quadratic beamforming for magnitude estimation," in *Proc. 29th European Signal Processing Conference, EUSIPCO-2021*, Aug 2021.

[13] B. Steinberg, *Principles of aperture and array system design: including random and adaptive arrays*. New York: Wiley, 1976.

[14] Z. He, F. Zheng, Y. Ma, H. H. Kim, Q. Zhou, and K. K. Shung, "A sidelobe suppressing near-field beamforming approach for ultrasound array imaging," *The Journal of the Acoustical Society of America*, vol. 137, no. 5, pp. 2785–2790, 2015.

[15] W. Y. Choi, S. W. Kwon, Y. H. Kim, K. C. Kang, and K. K. Park, "Single-shot near-field volumetric imaging system for optical ultrasound and photoacoustics using capacitive micromachined ultrasonic transducer without transmission mode," *IEEE Transactions on Ultrasonics, Ferroelectrics, and Frequency Control*, vol. 67, no. 6, pp. 1151–1158, 2020.

[16] M. E. Yanik and M. Torlak, "Near-field MIMO-SAR millimeter-wave imaging with sparsely sampled aperture data," *IEEE Access*, vol. 7, pp. 31 801–31 819, 2019.

[17] E. Grosicki, K. Abed-Meraim, and Y. Hua, "A weighted linear prediction method for near-field source localization," *IEEE Transactions on Signal Processing*, vol. 53, no. 10, pp. 3651–3660, 2005.

[18] P. Ioannides and C. Balanis, "Uniform circular and rectangular arrays for adaptive beamforming applications," *IEEE Antennas and Wireless Propagation Letters*, vol. 4, pp. 351–354, 2005.

[19] X. Chen, C. Pan, J. Chen, and J. Benesty, "Planar array geometry optimization for region sound acquisition," in *2021 IEEE International Conference on Acoustics, Speech and Signal Processing (ICASSP)*, 2021, pp. 756–760.

[20] K. Tan, S. Wu, Y. Wang, S. Ye, J. Chen, X. Liu, G. Fang, and S. Yan, "On sparse MIMO planar array topology optimization for UWB near-field high-resolution imaging," *IEEE Transactions on Antennas and Propagation*, vol. 65, no. 2, pp. 989–994, 2017.

[21] M. R. Bai, J.-H. Lin, and K.-L. Liu, "Optimized microphone deployment for near-field acoustic holography: To be, or not to be random, that is the question," *Journal of Sound and Vibration*, vol. 329, pp. 2809–2824, 7 2010.

[22] J. Chen, S. Chen, Y. Qi, and S. Fu, "Intelligent massive MIMO antenna selection using Monte Carlo tree search," *IEEE Transactions on Signal Processing*, vol. 67, no. 20, pp. 5380–5390, 2019.

[23] L. Yan, W. Huang, W. B. Kleijn, and T. D. Abhayapala, "Neural optimization of geometry and fixed beamformer for linear microphone arrays," in *ICASSP 2023 - 2023 IEEE International Conference on Acoustics, Speech and Signal Processing (ICASSP)*, 2023, pp. 1–5.

[24] J. H. Holland, "Genetic algorithms," *Scientific American*, vol. 267, pp. 66–73, 1992.

[25] A. Mohan and A. B. Raj, "Array thinning of beamformers using simple genetic algorithm," in *2020 International Conference on Computational Intelligence for Smart Power System and Sustainable Energy (CISPSSE)*, 2020, pp. 1–4.

[26] Y. Konforti, I. Cohen, and B. Berdugo, "Array geometry optimization for region-of-interest broadband beamforming," in *2022 International Workshop on Acoustic Signal Enhancement (IWAENC)*, 2022, pp. 1–5.

[27] G. Itzhak and I. Cohen, "Region-of-interest oriented constant-beamwidth beamforming with rectangular arrays," in *2023 IEEE Workshop on Applications of Signal Processing to Audio and Acoustics (WASPAA)*, 2023, pp. 1–5.

[28] M. R. Bai and C.-C. Chen, "Application of convex optimization to acoustical array signal processing," *Journal of Sound and Vibration*, vol. 332, no. 25, pp. 6596–6616, 2013.

[29] S. Boyd, S. P. Boyd, and L. Vandenberghe, *Convex optimization*. Cambridge university press, 2004.

[30] J. Martinez, N. Gaubitch, and W. B. Kleijn, "A robust region-based near-field beamformer," in *2015 IEEE International Conference on Acoustics, Speech and Signal Processing (ICASSP)*, 2015, pp. 2494–2498.

[31] W. Tager, "Near field superdirectivity (NFSD)," in *1998 IEEE International Conference on Acoustics, Speech and Signal Processing (ICASSP)*, vol. 4, 1998, pp. 2045–2048.

[32] I. McCowan, C. Marro, and L. Mauuary, "Robust speech recognition using near-field superdirective beamforming with post-filtering," in *2000 IEEE International Conference on Acoustics, Speech, and Signal Processing (ICASSP)*, vol. 3, 2000, pp. 1723–1726 vol.3.

[33] S. Diamond and S. Boyd, "CVXPY: A Python-embedded modeling language for convex optimization," *Journal of Machine Learning Research*, vol. 17, no. 83, pp. 1–5, 2016.

[34] M. ApS, *"MOSEK Optimizer API for Python 9.3.22"*, 2019. [Online]. Available: https://docs.mosek.com/9.3/pythonapi/index.html